Nuclear Instruments and Methods in Physics Research A 718 (2013) 126–129

Contents lists available at SciVerse ScienceDirect

Nuclear Instruments and Methods in Physics Research A

journal homepage: www.elsevier.com/locate/nima

# The AX-PET experiment: A demonstrator for an axial Positron Emission Tomograph

E. Bolle [a], C. Casella [b,*], E. Chesi [c], R. De Leo [d], G. Dissertori [b], V. Fanti [e], J.E. Gillam [f], M. Heller [g], C. Joram [g], W. Lustermann [b], E. Nappi [d], J.F. Oliver [f], F. Pauss [b], M. Rafecas [f], A. Rudge [c], U. Ruotsalainen [h], D. Schinzel [b,1], T. Schneider [g], J. Seguinot [g], P. Solevi [b], S. Stapnes [a], U. Tuna [h], P. Weilhammer [c]

[a] University of Oslo, NO-0317 Oslo, Norway
[b] ETH Zurich, CH-8092 Zurich, Switzerland
[c] Ohio State University, Columbus, OH 43210, USA
[d] INFN Sezione di Bari, I-70122 Bari, Italy
[e] Universitá e INFN Sezione di Cagliari, Cagliari, Italy
[f] IFIC, E-46071 Valencia, Spain
[g] CERN, PH Department, CH-1211 Geneva, Switzerland
[h] Tampere University of Technology, FI-33100 Tampere, Finland

ARTICLE INFO

Available online 7 August 2012

*Keywords:*
Positron Emission Tomography
PET
TOF-PET
LYSO scintillator
G-APD
SiPM
Digital SiPM

ABSTRACT

AX-PET stands for a new geometrical concept for a high resolution and high sensitivity PET scanner, based on an axial arrangement of long scintillating crystals in the tomograph, for a parallax free PET detector. Two identical AX-PET modules – consisting of matrices of LYSO crystals interleaved with WLS strips – have been built. They form the AX-PET Demonstrator, which has been extensively characterized and successfully used for the reconstruction of images of several phantoms. In this paper we report on the current status of the project, with emphasis on the most relevant results achieved both in terms of detector characterization and image reconstruction. We also discuss the recent preliminary results obtained with the digital SiPM from Philips (dSiPM), which are currently being tested as a possible alternative photodetector for AX-PET. With their very good intrinsic time resolution, dSiPM could add Time of Flight capability to the AX-PET concept.



## 1. Introduction

The AX-PET project [1,2] is a demonstrator of a novel geometrical approach to high resolution and high sensitivity Positron Emission Tomography (PET), in which long scintillator crystals (LYSO) are placed axially in the tomograph, in several layers, see Fig. 1. Arrays of plastic wave length shifter (WLS) strips, placed behind each layer of crystals, provide the measurement of the axial coordinate [3]. Such a compact arrangement of crystals and WLS strips allows for a precise 3D localization of the photon interaction point in the detector, with no parallax error. In the axial concept, the spatial resolution and the sensitivity are defined respectively by the transverse size of the chosen crystals and by the number of crystal layers. As such, they are completely independent one from the other and could in principle be both optimized at the same time. This is not the case in radial geometry PET, where the length of the crystals is a compromise between either a good spatial resolution (short crystals, which minimize the parallax error) or a high sensitivity (long crystals).

## 2. The AX-PET demonstrator

A demonstrator of the axial concept for a PET has been designed and built. It consists of two identical detector modules, used in coincidence. Each module comprises 48 LYSO crystals ($3 \times 3 \times 100\ mm^3$ each) and 156 WLS strips ($3 \times 0.9 \times 40\ mm^3$ each), arranged in six different layers, with eight crystals and 26 WLS strips per layer. Both the crystals and the WLS strips are individually read out by G-APDs (Geiger-mode Avalanche Photo Diodes). A fully analog readout chain is in charge of the processing of all channels, up to the digitization in a custom made ADC. An external trigger logic, based on the summed signals of all LYSO crystals in each of the two modules, forms the coincidences. With proper discriminating thresholds, the trigger selects events with a total energy deposition in the window [400, 600] keV in each module. Those events could be either

* Corresponding author. Tel./fax: +41 227673922; fax: +41 227671520.
*E-mail address:* Chiara.Casella@cern.ch (C. Casella).
[1] Now at Laboratory for Massachusetts Institute of Technology, Cambridge 02139, USA.

0168-9002/$ - see front matter © 2012 Elsevier B.V. All rights reserved.
http://dx.doi.org/10.1016/j.nima.2012.07.054

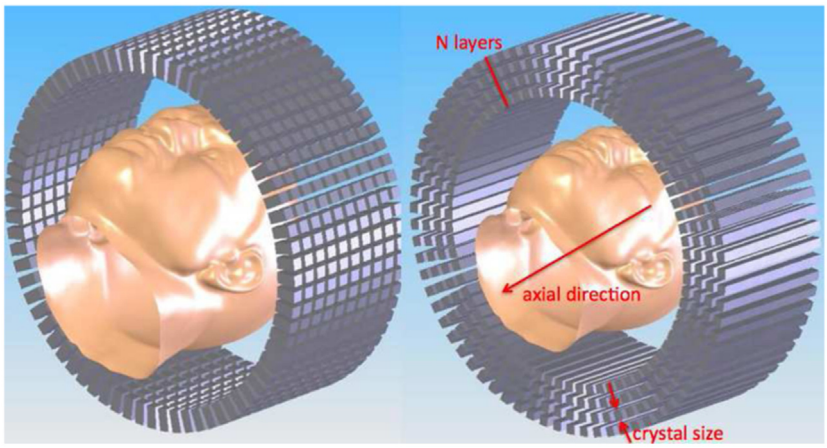


**Fig. 1.** Schematic illustration of the conventional radial geometry of a PET scanner (on the left) and of the novel axial arrangement of scintillator crystals, as proposed by AX-PET (on the right).

photoelectric absorptions (i.e., only one crystal hit in the module) or Compton scatterings followed by a photoelectric interaction (i.e. two or more hit crystals). Those inter-crystal scattering (ICS) events can be identified and eventually included in the reconstruction.

A detailed description of the design, performance and characterization of the various detector elements, up to the final construction of the AX-PET modules, is provided in Ref. [4].

## 3. AX-PET demonstrator results

### 3.1. Detector performance

The AX-PET demonstrator has been extensively characterized with point-like $^{22}$Na sources in several dedicated setups. It showed competitive performance, mainly in terms of spatial and energy resolutions. The measurement setups, procedures and results are described as well in Ref. [4]. We refer to this reference for further details.

- *Energy resolution*: Although a very good energy resolution is not mandatory in conventional PET scanners, it is obviously crucial for the identification of Compton scattering events. An energy resolution $\Delta E/E = 11.8\%$ (FWHM, at 511 keV), averaged over the 96 LYSO crystals of the two modules, is measured. This refers to energy calibrated spectra, already corrected also for the nonlinearity of the G-APDs (5% effect).
- *Spatial resolution*: In the transaxial plane, the detector spatial resolution is defined by the size of the adopted crystals: $R_{x,y} = \frac{3}{\sqrt{12}} \times 2.35 \sim 2$ mm, FWHM. In the axial direction, it is derived by the computation of the axial coordinate from the center of gravity method on the WLS strips, and it is measured to be $R_z \sim 1.8$ mm, FWHM. The confocal resolutions – when the two modules are used in coincidence – are $R_{x,y,coinc.} \sim 1.44$ mm, FWHM (derived from the size of the crystals) and $R_{z,coinc.} \sim 1.34$ mm, FWHM (measured).
- *Time resolution*: No timing information is accessible with the AX-PET readout. In a dedicated measurement on the summed signals of the modules operated in coincidence, a coincidence time resolution of $\sim 2$ ns FWHM is derived.

### 3.2. Image reconstruction

Once characterized in terms of its performance, the AX-PET demonstrator has been used for tomographic reconstructions of several different phantoms filled with $^{18}$F in water solution. Three different measurement campaigns have been performed, at the ETH[2] (April 2010) and at the AAA[3] (July 2010, July 2011). In order to acquire tomographic data (i.e., several projections at different angles), a special gantry setup was used, in which the source phantom was rotated in between the modules. To enlarge the field of view coverage, the modules were used both in the "face to face" configuration and in an oblique configuration, with one of the two modules rotated by 20°. Such a tomographic acquisition required long durations of the scans, which ultimately implied nonconstant operational conditions during the run (due to activity decay, accidental contributions, geometrical effects, etc.). A method based on the modeling of the count rate was developed to overcome such a limitation and adjust the acquisition duration in each position, to compensate for the count losses [5].

Dedicated AX-PET image reconstruction software has been developed. Different statistical iterative reconstruction approaches, based on the MLEM (Maximum Likelihood Expectation Maximization) technique, are used. A recent paper [6] describes the details of the various adopted reconstruction methods and shows the reconstructed images of several different phantoms. Among the most relevant results of the image reconstructions are:

- *NEMA-NU4 IQ* (*mouse*) *phantom*: The NEMA phantom includes five rod capillaries, with diameters 1, 2, 3, 4 and 5 mm, a uniformly filled chamber and two rods that could be filled independently with different activity concentrations, for the contrast assessment. In the reconstructed image, all five capillaries are correctly identified. Profiling the smallest one (1 mm, its size being smaller than the intrinsic resolution of the system), a width of 1.6 mm FWHM is measured. A good contrast is achieved between the rods filled with no and high activity concentration. A reasonably good uniformity is also achieved in the uniformly filled volume.
- *Custom made resolution phantom* (different sectors of different diameter rods, densely arranged in the phantom): The smallest diameter sector that could be reconstructed with a clear identification of all rods is 2.4 mm. A better quality of the image is obtained when the phantom is placed with the rods parallel to the axial direction.

[2] ETH Institute of Pharmaceutical Sciences, Animal Imaging Center - Zurich, Switzerland.

[3] Advanced Accelerator Applications, St Genis, France.

The images reconstructed and shown in Ref. [6] are obtained using only photoelectric absorption events. The inclusion of the ICS events in the same phantoms data is the subject of a recent work [7]. ICS events are considered if one unique interaction in one module and two interactions in the other occur. These "triple" ICS events result in two possible lines of response (LOR). In order to include them in the reconstruction, either both LORs can be used or one must be selected. Different approaches have been tested [7]. In general, the inclusion of ICS improved the image quality, at a small expense to resolution, and it is expected to have a bigger impact for small data sets.

### 3.3. Simulations

The AX-PET demonstrator has been fully modeled with dedicated Monte Carlo simulations, based on Geant4 and GATE. They have been developed specifically for the AX-PET application, mainly to include the nonconventional geometry of the scanner, an analytical modeling of the WLS behavior, and a dedicated sorter for the coincidences. AX-PET simulations have been used to support the characterization measurements, to test and optimize the image reconstruction software, and to train ICS identification and reconstruction algorithms. Simulations have been validated using the experimental data from the detector characterization measurements; the agreement between data and simulations is remarkably good [8].

## 4. Digital SiPM with the AX-PET

### 4.1. Philips digital SiPM

Digital Silicon Photomultipliers (dSiPM) [9,10] have been recently released by Philips. They are a fully digital implementation of Geiger mode avalanche photodiodes, in which each diode cell is integrated with conventional CMOS circuit on the same substrate. Each cell has its own readout circuit, which also provides an active quenching and the recharging, as well as a one memory bit used to selectively enable or disable the diode. Each diode of the sensors array is connected to a photon counter, which provides the number of detected photons, and to a TDC, for the registration of the arrival time of the triggering photons. Bypassing the process of propagation of analog signals, dSiPMs have a great potential in terms of reduced noise and time dispersion. Arrays of dSiPM have been developed [11]. We are using two different implementations, the DPC_6400-22-44 and the DPC_3200-22-44. In both cases, each device is an array of $8 \times 8$ dSiPM sensors; each sensor comprises 6400 or 3200 Geiger mode diode cells. In the terminology defined by Philips, each dSiPM sensor (counting 6400 or 3200 cells) is called *pixel* and the full device ($8 \times 8$ pixels) is called *tile*.

The capability of timestamp recording of the dSiPM, combined with the very good intrinsic time resolution of the dSiPM, makes those devices interesting in terms of a possible Time Of Flight (TOF) PET [12]. In a TOF-PET the time difference of the arrival of the two photons in the two opposite PET detectors is used to constrain the spatial position of the annihilation. As an example, a time difference of 100 ps would set the annihilation point at a distance of 1.5 cm from the center of the tomograph ($\Delta x = (c/2)\Delta t$). The limitation in localizing the annihilation point is obviously due to the time resolution of the coincidence system. While the present range of achieved time resolutions is not enough to directly identify the position of the annihilation, it has been shown that the signal-to-noise ratio (SNR) can be significantly improved in a TOF image.

Philips dSiPM are being tested as an alternative photodetector for AX-PET, in view of a possible TOF-PET detector module based on the axial concept. Its time performance – when coupled to long LYSO scintillator crystals – will be assessed. In addition, the axial coordinate reconstruction with the WLS strips coupled to dSiPM will be tested. A small scale dedicated setup, based on the AX-PET geometry and consisting of $2 \times 2$ LYSO crystals and 16 WLS strips ($2 \times 8$ i.e., eight strips in each of the two layers, covering only the central part of the crystals), is currently being built.

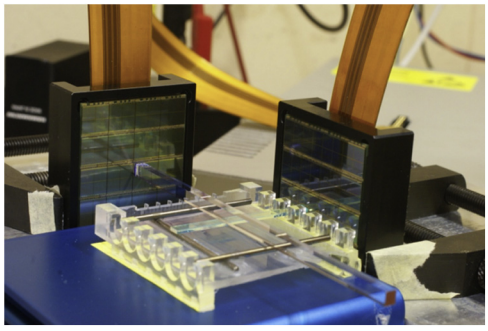

**Fig. 2.** Photograph of the "minimal AX-PET like setup" for preliminary tests of the dSiPM, in which one AX-PET LYSO crystal ($3 \times 3 \times 100\ \mathrm{mm}^3$) and one WLS strip ($3 \times 0.9 \times 40\ \mathrm{mm}^3$) are read out by two dSiPM tiles. The source (not shown in the photograph) is placed on top of the LYSO crystal.

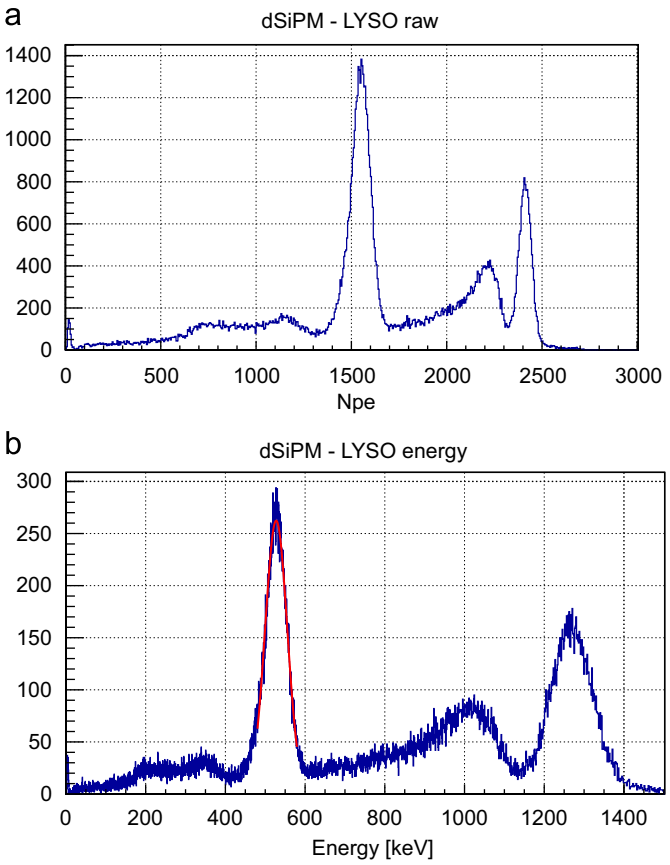


**Fig. 3.** Top: raw light yield spectrum of one AX-PET LYSO crystal exposed to photons from a $^{22}$Na source and coupled to one pixel of a dSiPM, DPC_3200-22-44. The raw spectrum – not corrected for the dSiPM saturation effects – directly represents the number of detected photoelectrons. Bottom: same calibrated and saturation corrected energy spectrum for the LYSO crystal.

### 4.2. Preliminary results with digital SiPM

As a preliminary test bench, a basic "minimal AX-PET like setup" has been assembled in which one LYSO crystal and one WLS strip – placed orthogonally behind it – are used to detect photons from a $^{22}$Na source (Fig. 2). Both the crystal and the WLS strip are coupled to two DPC_3200-22-44 tiles, using optical grease. Only one pixel per tile is enabled and the two tiles are acquired in coincidence. Good light yields are obtained, both for the LYSO ( $\sim$1500 pe at 511 keV, see Fig. 3) and for the WLS strip ( $\sim$50 pe in correspondence of the 511 keV energy deposition in the LYSO, see Fig. 4). After having applied the energy calibration to correct for the saturation effect of the dSiPM, a good energy resolution of $\sim$12.3% FWHM (at 511 keV) is measured, as also shown in Fig. 3.

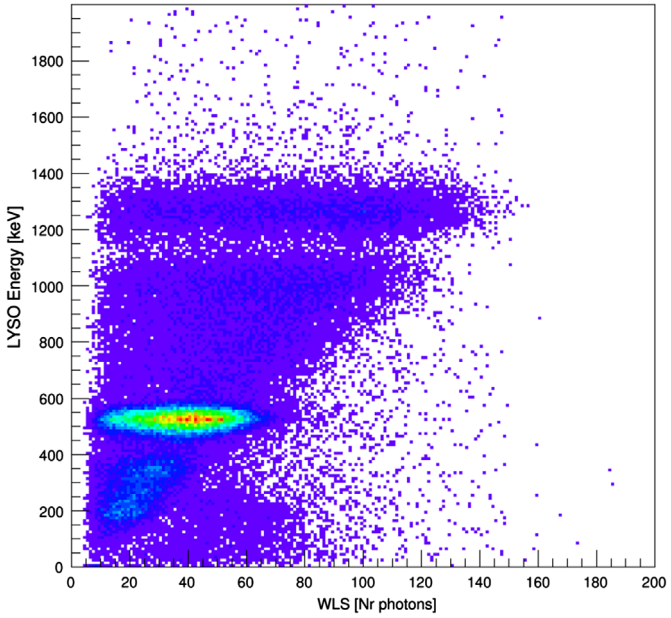


**Fig. 4.** Correlation between the energy deposition on the LYSO crystal (after energy calibration and saturation correction) and the light yield in the WLS strip of the minimal AX-PET like setup, when the LYSO crystal and WLS strip – coupled to dSiPM – are exposed to the $^{22}$Na source.

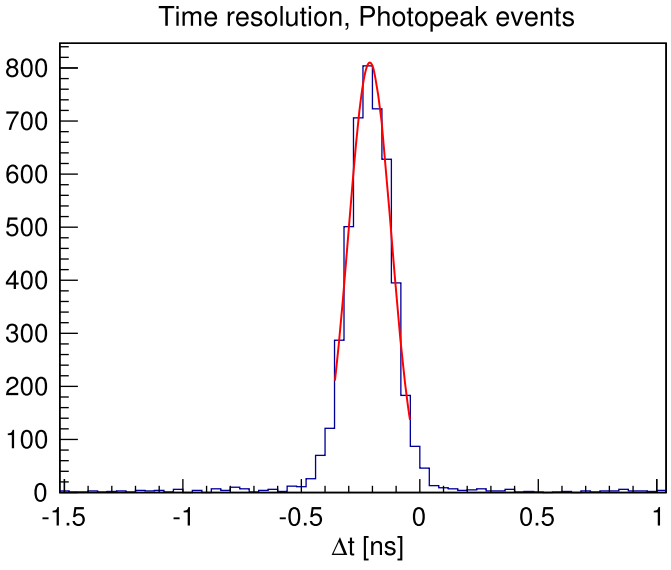


**Fig. 5.** Time difference in the arrival of the first triggering photon in two small dimensions LYSO crystals ($2\times2\times12$ mm$^3$), exposed to a $^{22}$Na source. The two crystals are coupled to two DPC_3200-22-44 dSiPM tiles, cooled with a Peltier unit down to 5 °C and acquired in coincidence. The plot refers to events with full energy deposition (511 keV, within resolution) in both crystals.

Preliminary results in terms of timing performance have also been obtained. For this measurement, two LYSO scintillator crystals of dimensions $2\times2\times12$ mm$^3$ (i.e. smaller than the AX-PET crystals) are coupled to two pixels of two different DPC_3200-22-44 tiles. The $^{22}$Na source is placed in between and the time difference in the arrival of the first photon in each one of the two tiles is measured, as shown in Fig. 5. In order to reduce the contribution of the dark count noise, which – when accidentally triggering – would give the wrong timing, the tiles are cooled down to 5 °C, using a Peltier unit. The optical coupling (with grease) and the quality of the adopted crystals are not optimized. Nevertheless, a very good coincidence timing resolution of about 200 ps FWHM is obtained.

## 5. Conclusions and perspectives

A demonstrator for a novel PET detector has been built, tested and fully characterized with $^{22}$Na sources. It has been successfully used for the reconstruction of images of several phantoms. The main novelties of the AX-PET – compared with standard PET solutions – are its geometry, with the axial arrangement of long LYSO crystals, and the WLS strips implementation for the axial coordinate measurement. Profiting of the high granularity of the detector module, combined with the individual readout of each crystal, inter-crystal scattering events (ICS) in the detector can be tagged and included in the reconstruction, contributing to an enhanced sensitivity of the detector. First tests in this direction are promising.

From the detector point of view, digital SiPM from Philips are currently being investigated as an alternative photodetector for the AX-PET. Preliminary results – achieved for the moment with rudimentary setups – show good time and energy resolution, indicating that dSiPMs may allow for compact detector modules with time of flight capability. This will be demonstrated in further measurements, in which the same detector components as used in the AX-PET (LYSO crystals and WLS strips) will be coupled to dSiPM.

In parallel with this development, a novel multichannel front-end electronics suitable for analog G-APD readout and compliant with the AX-PET requirements is being developed. Derived from the BASIC chip [13], already used with G-APD, the new chip is expected to achieve competitive timing performance.

## References

[1] J. Seguinot, et al., Il Nuovo Cimento C 29 (4) (2005) 429.
[2] A. Braem, et al., Nuclear Instruments and Methods in Physics Research Section A 580 (2007) 1513.
[3] A. Braem, et al., Nuclear Instruments and Methods in Physics Research Section A 586 (2008) 300.
[4] P. Beltrame, et al., Nuclear Instruments and Methods in Physics Research Section A 654 (2011) 546.
[5] E. Bolle, et al., in: NDIP 2011 Conference Proceedings, 2011 http://dx.doi.org/10.1016/j.nima.2011.12.114.
[6] P. Beltrame, et al., in: 2011 IEEE NSS Conference Record MIC 22-5, 2011.
[7] J. Gillam, et al., in: 2012 IEEE International Symposium on Biomedical Imaging, http://dx.doi.org/10.1109/ISBI.2012.6235484, in press.
[8] P. Solevi, et al., Proceedings of SPIE 7961 (2011) 796145.
[9] T. Frach, et al., in: 2009 IEEE NSS MIC Conference Record N28-005, 2009.
[10] T. Frach, et al., in: 2010 IEEE NSS MIC Conference Record N58-001, 2010.
[11] C. Degenhardt, et al., in: 2011 IEEE NSS MIC Conference Record, 2011, 10.1109/NSSMIC.2010.5874115.
[12] M. Conti, Physica Medica (25) (2009) 1.
[13] A. Argentieri, et al., Nuclear Instruments and Methods in Physics Research Section A 652 (2011) 516.